Technical Note	**LIGO-T1700322–v2**	2017/08/06

Searching for Echoes of Gravitational Waves from the Coalescence of Exotic Compact Objects: A Bayesian Approach
Second Interim Report

Rico Ka Lok Lo
The Chinese University of Hong Kong

Mentor:
Alan Weinstein
California Institute of Technology

Abstract

The ringdown part of the gravitational wave from the merger of two black holes was suggested as a probe of the internal structure of the remnant compact object, which may be more exotic than a black hole. Cardoso et al. pointed out that there would be a train of echoes in the late-time ringdown phase for different types of exotic compact objects (ECOs). Abedi et al. claimed that they have found evidence of echoes in binary black hole mergers detected by LIGO. In this project, we aim to search for echoes of gravitational waves in the three detections LIGO had, and verify their results using their phenomenological model with Bayesian analysis instead. We perform a Bayesian parameter estimation on the parameters related to echoes and Bayesian model selection of presence of echoes versus their absence, to provide stronger evidence for the presence or absence of echoes in these detections. The analysis technique developed in this project could be repeated with different models to provide even more robust evidence of the existence of echoes from ECOs.

1 Motivation and Objective

The ringdown part of the gravitational wave from the merger of two black holes was suggested as a probe of the internal structure of the remnant compact object, which may be more exotic than a black hole. Cardoso et al. pointed out that there would be a train of echoes in the late-time ringdown phase for different types of exotic compact objects (ECOs), which are the dampened reflection of waves emitted by the ECOs. It would be a major discovery if an exotic compact object is hiding inside a black hole. LIGO is uniquely capable of uncovering this because LIGO can observe the binary black hole merger, in which the coalescence of black holes with ECOs inside will generate echoes of gravitational wave in the ringdown phase.

Abedi et al. claimed that they have found evidence of echoes in binary black hole mergers detected by LIGO [5]. In this project, we aim to search for echoes of gravitational waves in the three detections LIGO had, and verify their results using their phenomenological model with Bayesian analysis instead. We perform a Bayesian parameter estimation on the parameters related to echoes and Bayesian model selection of presence of echoes versus their absence, to provide stronger evidence for the presence or absence of echoes in these detections. The analysis technique developed in this project could be repeated with different models to provide even more robust evidence of the existence of echoes from ECOs.

2 Background

As of this writing, the Laser Interferometer Gravitational-wave Observatory (LIGO) has successfully detected three compact binary coalescence events: GW150914, GW151226, GW170104 [2, 3, 4]. These detections mark the beginning of a new era of gravitational wave astronomy and astrophysics, where we can infer and probe the properties and struc-

ture of astronomical objects using gravitational-wave signals. Throughout the project, we will use geometrized unit $c = G = 1$.

2.1   Echoes of gravitational waves from coalescence of exotic compact objects

During the inspiral phase of gravitational wave emission from the coalescence of a compact binary system, for instance a binary black hole system, the two black holes spiral towards each other with an increasing orbital frequency. Eventually, they coalesce in the merger phase to form one single black hole. The final black hole then relaxes to a stationary Kerr black hole during the ringdown phase. Figure 1 shows the numerical relativity simulation and the reconstructed template of the first detection.
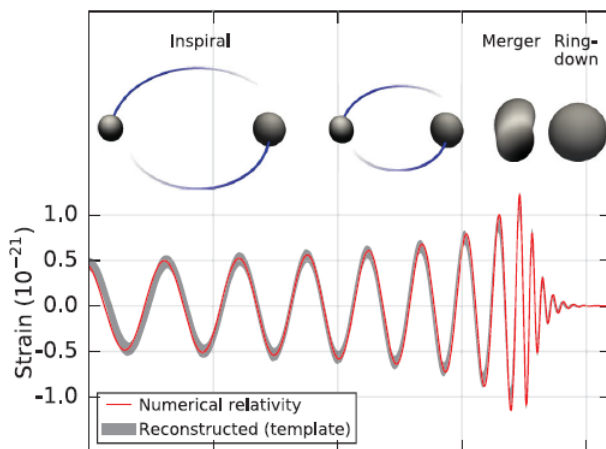

Figure 1: The numerical relativity simulation (in red) and reconstructed template (in gray) of GW150914. Figure taken from [3].

Cardoso, Franzin and Pani [8] first pointed out that the ringdown part of the gravitational wave can be used as a probe of the structure of a compact object. A very compact object, not necessary a black hole, with light ring will also exhibit similar ringdown as that of a black hole. Cardoso, Hopper, Macedo, Palenzuela and Pani [9] further showed that similar ringdown stage will also be exhibited for different types of **exotic compact objects** (ECOs) with light ring (or photon sphere), and there will be a train of echoes in the late-time ringdown phase associated with the photon sphere. Examples of ECOs are theoretical alternatives to black holes, such as gravastars[1] and fuzzballs. A common feature of these alternatives is that they replace the event horizon with a reflective surface. Figure 2 shows an example of the aforementioned echoes from a radially infalling particle into a wormhole in the ringdown phase.

2.1.1   Previous endeavours of searching the echoes of gravitational waves

2.1.1.1   Search and phenomenological model for echoes by Abedi et al.

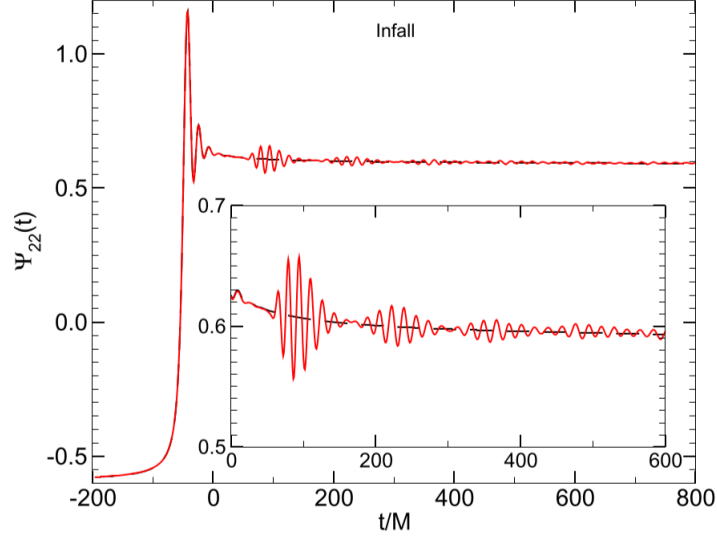[1]Gravastar stands for Gravitational Vacuum Star

Figure 2: The waveform of a radially infalling particle into a wormhole (in red) compared to that into a black hole (in black). We can clearly see the train of echoes for the wormhole case, whereas this feature is absent for black hole. Figure taken from [9].

Abedi, Dykaar and Afshordi published a paper on December 2016, claiming that they have found evidence of Planck-scale structure near the black hole event horizons at a combined 2.9σ significance level [5] on GW150914, LVT151012 and GW151226 using matched filtering technique.

In their search, they proposed a phenomenological model of echoes with 5 free parameters, with the phase change between each echo being π. The description of these 5 parameters are tabulated in Table 1.

Parameter	Description
Δt_{echo}	The time interval between each echo
t_{echo}	The time of arrival of the first echo
t_0	The time of truncation of the GW IMR template $\mathcal{M}_{\mathrm{I}}(t)$ to produce the echo template $\mathcal{M}_{\mathrm{TE,I}}(t)$
γ	The damping factor
A	The amplitude of the echoes relative to the IMR template

Table 1: The five free parameters of templates used by Abedi et al. [5].

Using the notations in [5], the echo template $\mathcal{M}_{\mathrm{TE,I}}(t)$ in time-domain is given by

$$\mathcal{M}_{\mathrm{TE,I}}(t) \equiv A \sum_{n=0}^{\infty} (-1)^{n+1} \gamma^n \mathcal{M}_{\mathrm{T,I}}(t)(t + t_{\mathrm{merger}} - t_{\mathrm{echo}} - n\Delta t_{\mathrm{echo}}, t_0), \tag{1}$$

where t_{merger} is the time of merger [2] and $\mathcal{M}_{\mathrm{T,I}}(t)$ is a smooth activation of the GW IMR[3] template given by

$$
\begin{aligned}
\mathcal{M}_{\mathrm{T,I}}(t) &\equiv \Theta(t, t_0)\mathcal{M}_{\mathrm{I}}(t) \\
&\equiv \frac{1}{2}\left\{1 + \tanh\left[\frac{1}{2}\omega_{\mathrm{I}}(t)(t - t_{\mathrm{merger}} - t_0)\right]\right\}\mathcal{M}_{\mathrm{I}}(t).
\end{aligned}
$$

Here $\omega_{\mathrm{I}}(t)$ denotes the angular frequency evolution of the IMR waveform as a function of time [5].

A team of physicists in Max Planck Institute for Gravitational Physics (AEI) questioned the data analysis method in Abedi et al.'s paper[7], especially the method to estimate the background and hence the statistical significance of the evidence they claimed. Abedi et al. responded that the shortcomings pointed by them would only change the significance by less than 0.3σ [6].

2.1.1.2 Phenomenological model by Nakano et al.

Motivated by solving the linear perturbation with a completely reflective boundary condition around a Kerr black hole, Nakano, Sago, Tagoshi and Tanaka suggested a refined phenomenological template of echoes of gravitational wave [19]. In frequency-domain, the template of the nth echo $\tilde{h}_n(f)$ is given by

$$
\tilde{h}_n(f) = e^{-i(2\pi f\Delta t + \phi(f))(n-1)}(\sqrt{R(f)})^{n-1}\sqrt{1 - R(f)} \quad \tilde{h}(f), \tag{2}
$$

where $\tilde{h}(f)$ is the Fourier transform of the waveform that reflects off the surface of ECO and $\phi(f)$ is the phase change when the gravitational wave was reflected at the potential barrier and at the boundary near horizon. The reflection rate, denoted by $\sqrt{R}$ in Eq.2, or reflection amplitude $\tilde{\mathcal{R}}_{\mathrm{BH}}$ (later defined in Eq.7), can be estimated using the fitting formulas in [19].

They also proposed two simple models of $h(t)$, the waveform that reflects off the surface of ECO, that we have just mentioned. The first model is given by

$$
h_1(t) \propto \frac{e^{-i\omega_{\mathrm{QNM}}\tilde{t}}}{1 + e^{-2\beta|\Im(\omega_{\mathrm{QNM}})|t}}, \tag{3}
$$

where $\beta \ll 1$ is a model parameter to eliminate the high frequency tail [19] due to the implicit periodic assumption when using Discrete Fourier Transform, and $\tilde{t}$ gives the frequency evolution, which is given by

$$
\frac{d\tilde{t}}{dt} = \frac{1}{1 + e^{-2\alpha|\Im(\omega_{\mathrm{QNM}})|t}}. \tag{4}
$$

---

[2]or equivalently time of coalescence, denoted by t_c
[3]IMR stands for **I**nspiral **M**erger **R**ingdown

As for the second model, it is given by

$$h_2(t) \propto \frac{e^{-i\omega_{\mathrm{QNM}}t}}{1 + e^{-2\bar{\alpha}|\Im(\omega_{\mathrm{QNM}})|t}}. \tag{5}$$

The two parameters α and $\bar{\alpha}$ are for controlling the excitation of quasi-normal mode at QNM frequency ω_{QNM} [19]. It should be noted that Nakano et al. claimed that the templates and reprocessing they proposed in [19] work in the context of gravitational-waves, namly

$$h(t) = h_+(t) + ih_\times(t),$$

where $h_+(t)$ and $h_\times(t)$ are the plus and cross polarization of gravitational waves respectively.

2.1.1.3 Phenomenological model by Mark et al.

Recently, Mark, Zimmerman, Du and Chen published a paper about the echoes from ECOs [17]. They modeled an exotic compact object with a Schwarzchild metric in the exterior and a spherically symmetric metric in the interior, together with a reflective boundary condition on the ECO surface $x = x_0$ with a reflection amplitude $\tilde{\mathcal{R}}(\omega)$. Here x is the tortoise coordinate defined as

$$x = r + 2M \ln(\frac{r - 2M}{M}).$$

They numerically calculated the scalar waves as observed by distant observers. They argued that the echo waveforms can be modulated from the waveform on the black hole horizon when there is no reflecting surface [17]. As such, they proposed a phenomenological template Z_{T} of the echoes from ECOs in frequency domain:

$$Z_{\mathrm{T}} = \tilde{K} Z_{\mathrm{T}}^{\mathrm{H}}, \tag{6}$$

where $Z_{\mathrm{T}}^{\mathrm{H}}$ is the horizon waveform template in frequency domain and $\tilde{K}$ is the transfer function, which contains most of the physics in this model. The transfer function $\tilde{K}(\omega)$, as a function of angular frequency ω, is given by

$$\tilde{K}(\omega) = \frac{\tilde{\mathcal{T}}_{\mathrm{BH}} \tilde{\mathcal{R}} e^{-2i\omega x_0}}{1 - \tilde{\mathcal{R}}_{\mathrm{BH}} \tilde{\mathcal{R}} e^{-2i\omega x_0}}, \tag{7}$$

where $\tilde{\mathcal{T}}_{\mathrm{BH}}(\omega)$, $\tilde{\mathcal{R}}_{\mathrm{BH}}(\omega)$ are the transmission amplitude and reflection amplitude of the black hole respectively, using the notations in [17]. Note that

$$|\tilde{\mathcal{T}}_{\mathrm{BH}}|^2 + |\tilde{\mathcal{R}}_{\mathrm{BH}}|^2 = 1.$$

We can expand Eq.7 as a geometric series:

$$\tilde{K}(\omega) = \tilde{\mathcal{T}}_{\mathrm{BH}} \tilde{\mathcal{R}} e^{-2i\omega x_0} \sum_{n=1}^{\infty} (\tilde{\mathcal{R}}_{\mathrm{BH}} \tilde{\mathcal{R}})^{n-1} e^{-2i(n-1)\omega x_0}. \tag{8}$$

If we define the transfer function for the nth echo as

$$\tilde{K}^{(n)} = (\tilde{\mathcal{T}}_{\mathrm{BH}} \tilde{\mathcal{R}})(\tilde{\mathcal{R}}_{\mathrm{BH}} \tilde{\mathcal{R}})^{n-1} e^{-2in\omega x_0}, \tag{9}$$

then we can write Eq.6 as a sequence of echoes

$$Z_\mathrm{T} = \sum_{n=1}^{\infty} Z_\mathrm{T}^{(n)} = \sum_{n=1}^{\infty} \tilde{K}^{(n)} Z_\mathrm{T}^\mathrm{H}.$$

The overall waveform observed by distant observers Z_ref^∞ is given by

$$Z_\mathrm{ref}^\infty = Z_\mathrm{BH}^\infty + \tilde{K} Z_\mathrm{BH}^\mathrm{H}.$$

Therefore, to generate a template for searching echoes, one just needs to add the reprocessed horizon template to the BH template in the frequency-domain.

Mark et al. observed that the ringdown of the horizon waveform determined the shape of the echoes. Hence, to get these features correct, Mark et al. proposed to use the following model [17]:

$$Z_\mathrm{T}^\mathrm{H}(\omega) = e^{i\omega t_s} e^{-\omega^2/(2\beta^2)} \left(\frac{\alpha_+}{\omega - \Omega_+} + \frac{\alpha_-}{\omega - \Omega_-} \right), \tag{10}$$

the meaning of the template parameters are tabulated in Table 2. Together with the surface of the ECO x_0, there are a total of five free parameters in this echo model.

Parameter	Description
α_+	The complex amplitude of the sinusoid at positive QNM frequency $\Omega_+ = \Omega_R + i\Omega_I$
α_-	The complex amplitude of the sinusoid at negative QNM frequency $\Omega_- = -\Omega_R + i\Omega_I$
t_s	The central start time of the Gaussian
β	The frequency width of the Gaussian

Table 2: The four free parameters of horizon templates used by Mark et al. [17].

2.2 Bayesian Analysis and Hypothesis Testing

Bayesian analysis provides us a consistent framework of inductive logic. The central piece of the Bayesian framework is the **Bayes' Theorem**, which allows us to update our degree of belief of a hypothesis H with a prior knowledge I when a new data d is available.

2.2.1 Bayes' Theorem

Mathematically, Bayes' theorem (also known as Bayes' rule) states that

$$\Pr(B|A) = \frac{\Pr(A|B)\Pr(B)}{\Pr(A)}, \tag{11}$$

where $\Pr(A)$ and $\Pr(B)$ denote the (discrete) probability of event A and event B occurs, regardless of each other, respectively; $\Pr(A|B)$ is the probability of event A **on the condition that** that event B occurs and likewise for $\Pr(B|A)$.

2.2.2 Parameter Estimation

Suppose we have a generative model H that describes the observed data d given some parameters $\vec{\theta} = (\theta_1, \theta_2, ..., \theta_n)$. Before the observation, suppose we already have some knowledge I about the parameters $\vec{\theta}$ assuming that the model H is true, represented by the **prior probability distribution** $p(\vec{\theta}|H, I)$, we can then use Eq.11 to update our knowledge or degree of belief of the value of these parameters to get the **posterior probability distribution** $p(\vec{\theta}|d, H, I)$ as follows:

$$p(\vec{\theta}|d, H, I) = \frac{p(d|\vec{\theta}, H, I)p(\vec{\theta}|H, I)}{p(d|H, I)} \tag{12}$$

$$= \frac{p(d|\vec{\theta}, H, I)p(\vec{\theta}|H, I)}{\int_\theta p(d|\vec{\theta'}, H, I)p(\vec{\theta'}|H, I)d\theta'}. \tag{13}$$

The term $p(d|\vec{\theta}, H, I)$, when viewed as a function of the parameters $\vec{\theta}$, is called the **likelihood** function and denoted as $\mathcal{L}(\vec{\theta}|d, H, I)$. As for the term $p(d|H, I)$, it is called the **evidence**, or marginal likelihood. In this scenario, it can be considered as a normalization constant and often ignored. Then, Eq.12 can be turned into:

$$p(\vec{\theta}|d, H, I) \propto p(d|\vec{\theta}, H, I)p(\vec{\theta}|H, I). \tag{14}$$

2.2.2.1 Parameter estimation in the context of GW

Suppose that the strain data $d(t)$ from a detector only consists of noise $n(t)$, which we assume to be Gaussian and stationary[4]. The probability that the noise $n(t)$ has a realization $n_0(t)$ (with zero mean) is given by [16]:

$$p(n_0) = \mathcal{N} \exp\left\{ -\frac{1}{2} \int_{-\infty}^{+\infty} df \frac{|\tilde{n}_0(f)|^2}{(1/2)S_n(f)} \right\}, \tag{15}$$

where $\mathcal{N}$ is a normalization constant and $S_n(f)$ is the power spectrum density of noise. If we introduce the notion of **noise-weighted inner product**, namely

$$(A|B) = 4\Re \int_0^\infty df \frac{\tilde{A}^*(f)\tilde{B}(f)}{S_n(f)}, \tag{16}$$

then we can rewrite Eq. 15 into

$$p(n_0) = \mathcal{N} \exp\left\{ -\frac{1}{2}(n_0|n_0) \right\}. \tag{17}$$

---

[4]A stationary random process means that the statistical properties of the process do not change with time [10].

Suppose the strain data $d(t)$ consists of both noise $n_0(t)$ and GW signal $h(t; \vec{\theta})$, namely

$$n_0(t) = d(t) - h(t; \vec{\theta}),$$

then the the likelihood $p(d|\vec{\theta}, H, I)$ for single detector can be obtained from Eq. 15:

$$p(d|\vec{\theta}, H, I) = \mathcal{N} \exp\left\{-\frac{1}{2}(d(t) - h(t; \vec{\theta})|d(t) - h(t; \vec{\theta}))\right\}. \tag{18}$$

For the case of multiple detectors, if we assume that the noise distributions are all Gaussian and stationary, and more importantly independent of each other, then we have

$$p(d_{\mathrm{H1}}, d_{\mathrm{L1}}|\vec{\theta}, H, I) = \prod_{i \in \{H1, L1\}} \mathcal{N}_i \exp\left\{-\frac{1}{2}(d_i(t_i) - h(t_i; \vec{\theta})|d_i(t_i) - h(t_i; \vec{\theta}))\right\}. \tag{19}$$

For computational reasons, it is often easier to deal with **log prior**, **log likelihood** and **log posterior**. In particular, Eq. 12 for posterior distribution becomes

$$\ln p(\vec{\theta}|d, H, I) = \ln p(d|\vec{\theta}, H, I) + \ln p(\vec{\theta}|H, I) - \ln p(d|H, I). \tag{20}$$

If we substitute the likelihood function into Eq. 20, we have

$$\ln p(\vec{\theta}|d, H, I) = -\frac{1}{2}(d(t) - h(t; \vec{\theta})|d(t) - h(t; \vec{\theta})) + \ln p(\vec{\theta}|H, I) + \ln K, \tag{21}$$

where K is a constant independent of $\vec{\theta}$.

After we have sampled the posterior distribution, for example by means of Markov Chain Monte Carlo discussed in Section 2.3, we can calculate various estimators as point estimates, such as maximum likelihood estimator (MLE), which is

$$\hat{\theta}_{\mathrm{MLE}} = \arg\max \mathcal{L}(\vec{\theta}|d, H, I).$$

Another estimator is maximum a posteriori estimator (MAP), which is

$$\hat{\theta}_{\mathrm{MAP}} = \arg\max p(\vec{\theta}|d, H, I).$$

Note that these two estimators would change if one marginalizes over some parameters. On the other hand, the Bayes estimator, which is essentially the mean value of $\vec{\theta}$, is invariant to marginalization, namely

$$\hat{\theta}_{\mathrm{Bayes}} = \int \vec{\theta} p(\vec{\theta}|d, H, I) d\vec{\theta}.$$

2.2.3 Hypothesis Testing

Suppose we have two (generative) models H_0 and H_1, and we want to compare which model describes the observed data the best. It is useful to compute the **odds ratio** defined as

$$O_{H_0}^{H_1} = \frac{p(H_1|d, I)}{p(H_0|d, I)}. \tag{22}$$

Applying Eq.11 to Eq.22, we have

$$O_{H_0}^{H_1} = \frac{p(d|H_1, I)p(H_1|I)}{p(d|H_0, I)p(H_0|I)}.$$

The factor $\dfrac{p(H_1|I)}{p(H_0|I)}$ is called the **prior odds** and the factor $\dfrac{p(d|H_1, I)}{p(d|H_0, I)}$ is called the **Bayes factor**, denoted as $B_{H_0}^{H_1}$.

A question that arises naturally is that how can we compute the term $p(d|H_i, I)$, where $i = 0, 1$. Suppose H_0 has no free parameter, whereas H_1 has n free parameters $\vec{\theta} = (\theta_1, \theta_2, ..., \theta_n)$. Then it is straightforward to calculate $p(d|H_0, I)$. But for $p(d|H_1, I)$, by re-arranging Eq.11 we have

$$p(\vec{\theta}|d, H_1, I)p(d|H_1, I) = p(d|\vec{\theta}, H, I)p(\vec{\theta}|H_1, I).$$

Integrating both sides with respect to $\vec{\theta}$ (or *marginalizing over the parameters*), we have

$$\int p(\vec{\theta}|d, H_1, I)p(d|H_1, I)d\vec{\theta} = \int p(d|\vec{\theta}, H_1, I)p(\vec{\theta}|H_1, I)d\vec{\theta}.$$

Note that $p(d|H_1, I)$ is independent of $\vec{\theta}$ and by definition

$$\int p(\vec{\theta}|d, H_1, I)d\vec{\theta} = 1,$$

We finally arrive at

$$p(d|H_1, I) = \int p(d|\vec{\theta}, H_1, I)p(\vec{\theta}|H_1, I)d\vec{\theta}. \tag{23}$$

When the odds ratio $O_{H_0}^{H_1} > 1$, that means the observed data favors (alternative) hypothesis H_1 more than the hypothesis H_0 and vice versa.

One thing that we must be cautious about is that a model that fits the data best does not imply the model gives the highest evidence. A more complicated model (i.e. with more free parameters) often subjects to more noise than a simpler model (i.e. with less free parameters). This is similar to over-fitting in regression. When you have N data points for fitting, you can always use a degree N polynomial to fit all points, but very likely the fitted polynomial will not generalize well to new data because it was affected by the noise in the data.

Bayesian analysis embodies the **Occam's razor** and penalizes more complicated models automatically. The following example was taken from [15]. Suppose there are two models H_0 and H_1 with H_0 having no free parameter and H_1 having 1 free parameter θ. Assume that there is no prior knowledge to favor a particular model, i.e. the prior odds is simply 1. We further assume that the prior probability distribution for model H_1 is constant over a range $\theta \in [\theta_{\min}, \theta_{\max}]$, namely

$$p(\theta|H_1, I) = \begin{cases} \dfrac{1}{\theta_{\max} - \theta_{\min}}, & \theta \in [\theta_{\min}, \theta_{\max}] \\ 0, & \text{otherwise} \end{cases}.$$

We also assume that the likelihood to be a Gaussian function, centered around the maximum likelihood when $\theta = \theta_0$, with a standard deviation of σ_θ. Mathematically,

$$p(d|\theta, H_1, I) = p(d|\theta_0, H_1, I)e^{-\frac{(\theta - \theta_0)^2}{2\sigma_\theta^2}}.$$

The odds ratio can be found easily by integration:

$$O_{H_0}^{H_1} = \frac{p(d|\theta_0, H_1, I)}{p(d|H_0, I)}\frac{\sqrt{2\pi}\sigma_\theta}{\theta_{\max} - \theta_{\min}}.$$

Very often, the first factor $\dfrac{p(d|\theta_0, H_1, I)}{p(d|H_0, I)} > 1$, since often a more complicated model fits the noisy data better than a simpler model. However, the second factor suggests that if the parameter θ is unnecessary to describe the data in a sense that the width of the likelihood function is much smaller than the width of the prior, i.e. $\sigma_\theta \ll \theta_{\max} - \theta_{\min}$, the second factor will penalize H_1 is a sense that the odds ratio will become smaller.

2.3   Markov Chain Monte Carlo (MCMC)

In Section 2.2.2 and 2.2.3, we outlined the procedures of performing parameter estimation and hypothesis testing respectively. To perform the actual Bayesian analysis, we would need to sample from the posterior distribution $p(\vec{\theta}|d, H, I)$. Markov Chain Monte Carlo (MCMC) is the standard tool to complete this task.

A Markov chain of random variables $\{x_1, x_2, ..., x_N\}$ satisfies the property

$$\Pr(x_{i+1}|x_1, x_2, ..., x_i) = \Pr(x_{i+1}|x_i).$$

That is, the probability of transiting from x_i to x_{i+1} depends on the current state x_i only. Suppose we want to draw samples from the distribution $\pi(x)$. To make sure that the Markov chain will converge to the target distribution $\pi(x)$, the target distribution needs to be stationary, i.e.

$$\pi(x') = \int \pi(x)q(x, x')dx, \tag{24}$$

and detailed balance, i.e.

$$\pi(x)q(x, x') = \pi(x')q(x', x), \tag{25}$$

where $q(x, x')$ is called the transition kernel, and

$$\Pr(x_i|x_1, x_2, ..., x_{i-1}) = \int q(x_{i-1}, x)dx.$$

If the posterior distribution that we desire satisfies the above conditions, then we are in a good shape to utilize MCMC.

2.3.1   Metropolis and Metropolis-Hasting algorithm

2.3.1.1   Metropolis algorithm

Metropolis algorithm is the simplest and earliest algorithm for MCMC, proposed by Metropolis and Ulam [18] in 1949. Here we outline the Metropolis algorithm. For the sake of simplicity, we denote the posterior distribution as $\mathcal{P}$.

1. Initialize $\vec{\theta}_{i=0}$

2. Propose a jump $\vec{\delta\theta} = (\theta_{\text{proposed},n} - \theta_{i-1,n})$ according to the proposal distribution, i.e. $\delta\theta_n \sim \Lambda_n$

3. Accept the jump $\vec{\theta}_i = \vec{\theta}_{\text{proposed}}$ with a probability of $\min(\frac{\mathcal{P}_{\text{proposed}}}{\mathcal{P}_{i-1}}, 1)$. Else set $\vec{\theta}_i = \vec{\theta}_{i-1}$

4. Repeat step 2 & 3 for a sufficient amount of steps

5. Discard early steps (also known as burn-in)

Note that there are hyperparameters controlling the proposal distribution. A common choice of the proposal distribution is a multivariate Gaussian distribution, i.e.

$$\Lambda_n = N(0, \sigma_n^2),$$

where σ_n is the standard deviation of the distribution in the nth dimension and it is a hyperparameter of the MCMC algorithm. Albeit its simplicity, the power of Metropolis algorithm is limited in a sense that the proposal distribution Λ_i in this algorithm cannot be asymmetric, which can be problematic when sampling anisotropic distributions. Also the algorithm converges slowly. To solve these problems, we can use the updated version called Metropolis-Hasting algorithm.

2.3.1.2 Metropolis-Hasting algorithm

Metropolis-Hasting algorithm is very similar to Metropolis algorithm, proposed by Hasting [14] in 1970. However, this algorithm does not require a symmetric proposal distribution. Here we outline the Metropolis-Hasting algorithm.

1. Initialize $\vec{\theta}_{i=0}$

2. Propose a jump $\vec{\delta\theta} = (\theta_{\text{proposed},n} - \theta_{i-1,n})$ according to the proposal distribution, i.e. $\delta\theta_n \sim \Lambda_n$

3. Accept the jump $\vec{\theta}_i = \vec{\theta}_{\text{proposed}}$ with a probability of $\min(\frac{\mathcal{P}_{\text{proposed}}}{\mathcal{P}_{i-1}} \frac{\Lambda(\vec{\theta}_{\text{proposed}}|\vec{\theta}_{i-1})}{\Lambda(\vec{\theta}_{i-1}|\vec{\theta}_{\text{proposed}})}, 1)$. Else set $\vec{\theta}_i = \vec{\theta}_{i-1}$

4. Repeat step 2 & 3 for a sufficient amount of steps

5. Discard early steps (also known as burn-in)

A common issue with Metropolis/Metropolis-Hasting algorithm is that it cannot sample multi-modal distributions well. This problem can be overcome by parallel tempering, or replica exchange.

2.3.2 Parallel tempering

Parallel tempering, or replica exchange, was originally proposed by Swendsen and Wang [20] in 1986. The idea is that we have N different chains running MCMC at different temperatures T in parallel with slightly modified likelihood function

$$p(d|\vec{\theta}, H, I, \beta) = \left[p(d|\vec{\theta}, H, I) \right]^{\beta}, \tag{26}$$

where $\beta \equiv \frac{1}{T}$. Note that $T = 1$ chain must be present, since this is the chain that contains the desired posterior samples.

During the run, chains of different temperatures swap samples with some criteria [20]. This is desirable because the hotter chain has a flatter likelihood, and hence it can explore the parameter space more easily, whereas the cooler chain explores a local maximum well. This can help us sample multi-modal distributions. However, the purpose of using parallel tempering is not for sampling multi-modal distributions, since we expect the joint-posterior distribution for the parameters should be unimodal. The reason why we adopt parallel tempering sample in this project is for the estimation of evidence, which is essential to model selection.

2.3.2.1 Thermodynamic integration

From Eq. 23 that the evidence is given by

$$p(d|H_1, I) = \int p(d|\vec{\theta}, H_1, I) p(\vec{\theta}|H_1, I) d\vec{\theta}.$$

When performing the thermodynamic integration, derived in [13], we introduce a new quantity which depends on β:

$$p(d|H_1, I, \beta) = \int [p(d|\vec{\theta}, H_1, I)]^{\beta} p(\vec{\theta}|H_1, I) d\vec{\theta}. \tag{27}$$

Consider

$$\begin{aligned}
\frac{d\ln p(d|H_1, I, \beta)}{d\beta} &= \frac{d\ln p(d|H_1, I, \beta)}{dp(d|H_1, I, \beta)} \frac{dp(d|H_1, I, \beta)}{d\beta} \\
&= \frac{1}{p(d|H_1, I, \beta)} \frac{d}{d\beta} \int [p(d|\vec{\theta}, H_1, I)]^{\beta} p(\vec{\theta}|H_1, I) d\vec{\theta} \\
&= \frac{1}{p(d|H_1, I, \beta)} \int \ln p(d|\vec{\theta}, H_1, I) [p(d|\vec{\theta}, H_1, I)]^{\beta} p(\vec{\theta}|H_1, I) d\vec{\theta} \\
&= \left\langle \ln p(d|\vec{\theta}, H_1, I) \right\rangle_{\beta},
\end{aligned}$$

where $\langle \cdots \rangle_{\beta}$ denotes the average with respect to the posterior distribution at $T = \frac{1}{\beta}$. Then by integration, we have

$$\ln p(d|H_1, I, \beta) = \int \left\langle \ln p(d|\vec{\theta}, H_1, I) \right\rangle_{\beta} d\beta. \tag{28}$$

Note that ultimately we want $p(d|H_1, I, \beta = 1)$, the evidence, and by definition

$$p(d|H_1, I, \beta = 0) = \int p(\vec{\theta}|H_1, I)d\vec{\theta} = 1.$$

Therefore, the natural choice of the lower and upper bound for evaluating Eq. 28 would be 0 and 1 respectively, also for the LHS of Eq. 28,

$$\ln p(d|H_1, I, \beta = 1) - \ln p(d|H_1, I, \beta = 0) = \ln p(d|H_1, I).$$

Finally, we have

$$\ln p(d|H_1, I) = \int_0^1 \left\langle \ln p(d|\vec{\theta}, H_1, I) \right\rangle_\beta d\beta. \tag{29}$$

Since in parallel tempering we have chains with different values of β, we can estimate the integral in Eq. 29 easily.

3 Progress and Challenges encountered

3.1 Implementing templates of echoes

3.1.1 Phenomenological model by Mark et al.

As part of the work, the template model described in [17] by Mark et al. was implemented in Python. Table 3 summarizes the seven main functions in the implementation `phenom_echoes_waveform_tapir.py`.

Function	Description
`get_fd_horizon_waveform`	Generate the horizon waveform in frequency-domain $Z_{\mathrm{T}}^{\mathrm{H}}$
`get_fd_total_transfer`	Compute the total transfer function $\tilde{K}$
`get_fd_nth_transfer`	Compute the nth transfer function $\tilde{K}^{(n)}$
`get_fd_total_echoes`	Generate the total echo waveform in frequency-domain Z_{T}
`get_td_total_echoes`	Generate the total echo waveform in time-domain $\psi(t)$ by performing Fourier Transform on the frequency-domain waveform: $$\psi(t) = \int_{-\infty}^{+\infty} \frac{d\omega}{2\pi} Z(\omega)e^{-i\omega t} \tag{30}$$
`get_fd_up_to_n_echoes`	Generate the echo waveform up to n^{th} echo in frequency-domain $Z_{\mathrm{T}} = \sum_{k=1}^n Z_{\mathrm{T}}^{(k)}$
`get_td_up_to_n_echoes`	Generate the echo waveform up to n^{th} echo in time-domain by performing Fourier Transform to the frequency-domain waveform

Table 3: The seven main functions in the Python implementation of template model described in Mark et al. [17].

3.1.2 Computing the reflection amplitude $\tilde{\mathcal{R}}_{\text{BH}}(\omega)$ and transmission amplitude $\tilde{\mathcal{T}}_{\text{BH}}(\omega)$

In both Nakano et al.'s and Mark et al.'s models, there are two quantities that are required: reflection amplitude $\tilde{\mathcal{R}}_{\text{BH}}(\omega)$ in Mark et al.'s notation or $\sqrt{R}$ in Nakano's notation, and transmission amplitude $\tilde{\mathcal{T}}_{\text{BH}}(\omega)$ in Mark et al.'s notation or $\sqrt{1-R}$ in Nakano's notation. From now on, we will use Mark et al.'s notations for the sake of clarity and consistency.

In Nakano et al.'s paper, there are two fitting formulas for $\tilde{\mathcal{R}}_{\text{BH}}$, one for positive and one for negative frequencies f. In practice, we would need to compute the reflection amplitude (and hence transmission amplitude by the normalization condition) for each of the systems LIGO had detected. For now, we will be using Nakano et al.'s fit for testing purposes to build the infrastructure of the search pipeline first. Figure 3 shows a plot of the reflection and transmission amplitude fit described in [19] for positive frequency f, parameterized by $x = 2\pi M f$ and q, where M is the mass of the black hole and q is the dimensionless spin parameter.
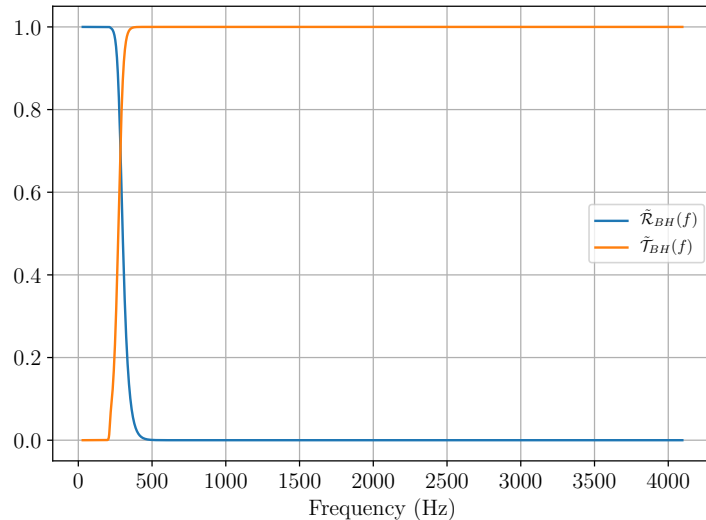

Figure 3: Nakano et al.'s fit for reflection and transmission amplitude as a function of frequency f, using the final mass and spin of the black hole given in [3] for the GW150914 event.

3.1.3 Using Mark et al.'s model in the context of GW

In Section 2.1.1, we mentioned that Nakano et al. argued that their templates work in the context of gravitational waves. However, attention must be paid when using the template proposed by Mark et al., since they derived the results in the context of scalar waves, whereas gravitational waves are metric perturbations from Minkowski spacetime $h_{\mu\nu} = g_{\mu\nu} - \eta_{\mu\nu}$. Also, the template was derived using a Schwarzchild spacetime, but the sources of LIGO's three detections are all rotating instead of static. Therefore, the template becomes

a phenomenological model when we try to extend it to the case of gravitational waves from rotating ECOs.

For an observer far away ($r \to \infty$), the Weyl scalar Ψ_4 relates to the second time derivative of the gravitational waves as

$$\Psi_4 = \ddot{h}_+ - i\ddot{h}_\times. \tag{31}$$

We **claim** (or rather *hope*) that template for modeling ψ proposed by Mark et al. also models Ψ_4. That means we can generate echo templates for gravitational waves by performing double integration with respect to time from the TAPIR templates for scalar fields.

From Eq. 6 and Eq. 30, we have

$$\psi_{\mathrm{echo}}(t) = \int_{-\infty}^{+\infty} \frac{d\omega}{2\pi} Z_{\mathrm{echo}}(\omega) e^{-i\omega t}.$$

Note that the only time dependence is in the term $e^{-i\omega t}$, that means double integration in time is equivalent to dividing the frequency waveform Z_{echo} by $(-i\omega)^2 = -\omega^2$. Hence, we have

$$h_+(t) - ih_\times(t) = \int_{-\infty}^{+\infty} \frac{d\omega}{2\pi} \frac{Z_{\mathrm{echo}}(\omega)}{-\omega^2} e^{-i\omega t}. \tag{32}$$

Since we are doing analysis on a *finite segment* of data, we must truncate the echo waveform, up to N^{th} echo, as follows

$$
\begin{aligned}
h_+(t) - ih_\times(t) &= \sum_{n=1}^{N} \int_{-\infty}^{+\infty} -\frac{d\omega}{2\pi\omega^2} \tilde{K}^{(n)} Z_{\mathrm{T}}^{\mathrm{H}}(\omega) e^{-i\omega t} \\
&= \sum_{n=1}^{N} \int_{-\infty}^{+\infty} -\frac{d\omega}{2\pi\omega^2} (\tilde{\mathcal{T}}_{\mathrm{BH}}\tilde{\mathcal{R}})(\tilde{\mathcal{R}}_{\mathrm{BH}}\tilde{\mathcal{R}})^{n-1} e^{-i\omega(t-t_s+2nx_0)} e^{-\omega^2/(2\beta^2)} \left(\frac{\alpha_+}{\omega - \Omega_+} + \frac{\alpha_-}{\omega - \Omega_-} \right)
\end{aligned}
$$

We examine the term $e^{-i\omega(t-t_s+2nx_0)}$, it implies that the first echo starts roughly at $t = t_s + 2|x_0|$, and each successive echo is $2|x_0|$ apart. Note that we can infer the **compactness** of the ECO from the value of $|x_0|$.

3.1.4   Echo template for GW150914 using Mark et al.'s model

To demonstrate that we could use Mark et al.'s model to search for echoes of gravitational waves, we have generated a template with echoes for GW150914, the loudest event among the three we had. The QNM frequencies $\Omega_\pm$ for the horizon waveform used for generating this echo template was constructed using the least-damped QNM ($l = 2, m = 2$ mode) of the event, taken from [1], namely

$$\Omega_\pm = \pm 502\pi + i\frac{-1}{4.0 \times 10^{-3}}.$$

Figure 4a and 4b show the frequency-domain and time-domain horizon waveform for generating the echoes in GW150914 respectively. Using Nakano et al.'s fitting of $\tilde{\mathcal{R}}_{\mathrm{BH}}(f)$, $\tilde{\mathcal{T}}_{\mathrm{BH}}(f)$,

and assuming that the reflectivity $\tilde{R}$ of the ECO surface is frequency-independent, we were able to generate a template for echoes in GW150914. Figure 5a and 5b show the best-fit IMR waveform of GW150914 with three echoes appended and the three echoes respectively in time domain.
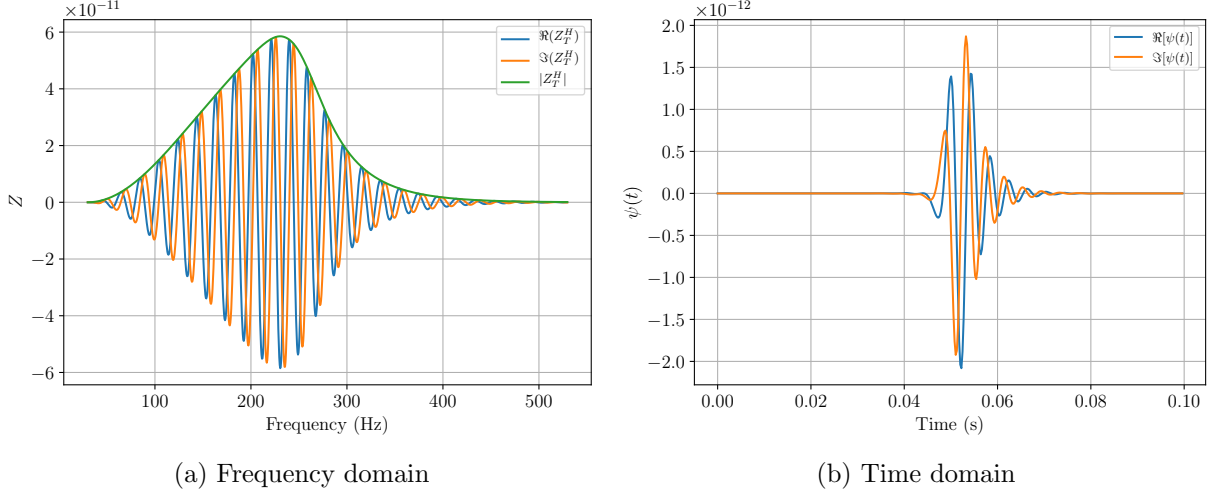

(a) Frequency domain   (b) Time domain

Figure 4: The horizon waveform for generating the echoes in GW150914.

3.1.5 Phenomenological model by Abedi et al.

As part of the work, the template model described in [5] by Abedi et al. was implemented in Python. Table 4 summarizes the five main functions in the implementation `phenom_echoes_waveform_abedi.py`.

Function	Description
`get_td_ligo_template`	Generate the IMR template in time domain. Currently it is a wrapper of `pycbc.waveform.get_td_waveform` in PyCBC
`get_frequency_evolution`	Compute the frequency evolution of the IMR template $\omega_I(t)$. Currently it is a wrapper of `waveform.utils.frequency_from_polarizations` in PyCBC
`get_td_cutoff`	Compute the cut-off function $\Theta(t, t_0)$
`get_td_echo_up_to_n`	Generate the echo waveform up to n^{th} echo in time-domain
`get_fd_echo_up_to_n`	Generate the echo waveform up to n^{th} echo in frequency-domain by performing Fourier transform on the time-domain template

Table 4: The five main functions in the Python implementation of template model described in Abedi et al. [5].
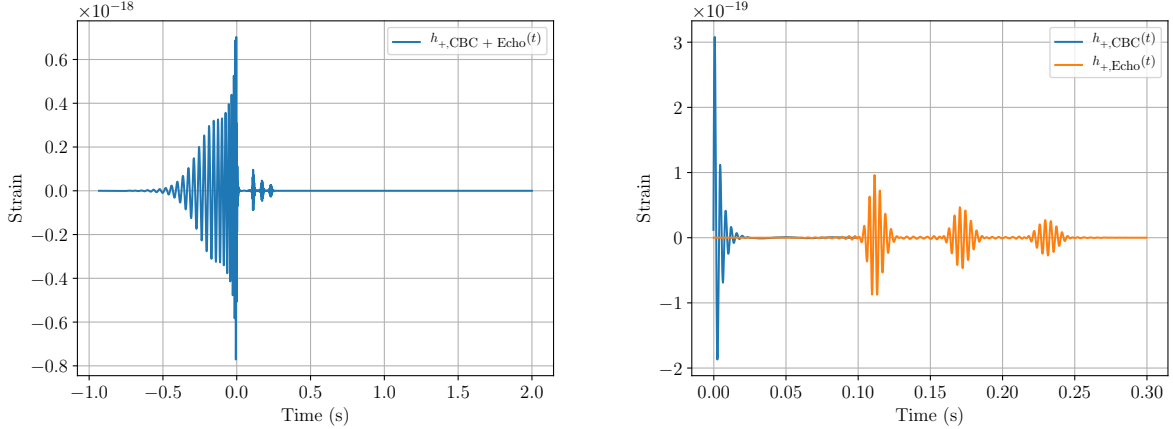
(a) GW150914 best-fit IMR waveform with three echoes appended

(b) The train of echoes, with $n = 3$

Figure 5: The best-fit IMR time-domain template GW150914 with three echoes in the source frame.

To demonstrate that we could use Abedi et al.'s model to search for echoes of gravitational waves, we have generated a template with echoes for GW150914. Figure 6a and 6b shows the frequency evolution $\omega_I(t)$ of the best-fit IMR template of GW150914 and smooth cut-off function $\Theta(t, t_0)$ to be applied to the IMR waveform to produce the echo waveform respectively. Figure 7a and 7b show the best-fit IMR time-domain waveform of GW150914 with three echoes appended and the truncated IMR time-domain waveform $\mathcal{M}_{\mathrm{T,I}}(t)$ used to generate the echo template respectively in the source frame.

3.2   Bayesian analysis on fake strain data

Before performing the Bayesian analysis on actual strain data, it is educational to perform the same analysis on fake strain data first, namely strain data with Gaussian noise and IMR signal with echoes (which we will refer as *IMRE*) of known parameters. By recovering the injected signal and inferring the parameters correctly, we can learn that the analysis method proposed would be able to find signals in real strain data, and that the method has been properly implemented.

3.2.1   Generating fake strain data

In order to generate fake strain data, a program `generate_fake_strain.py` was written in Python. The power spectrum density used to produce the noise here is the analytical PSD `aLIGOZeroDetHighPower`. To generate the IMRE strain $h_{\mathrm{H1/L1}}(t)$ in detector frame from the plus and cross polarizations $h_+(t)$, $h_\times(t)$ in source frame, note that

$$h_{\mathrm{H1/L1}}(t) = F_{+,\mathrm{H1/L1}}(t; \alpha, \delta, \psi) h_+(t) + F_{\times,\mathrm{H1/L1}}(t; \alpha, \delta, \psi) h_\times(t), \tag{33}$$
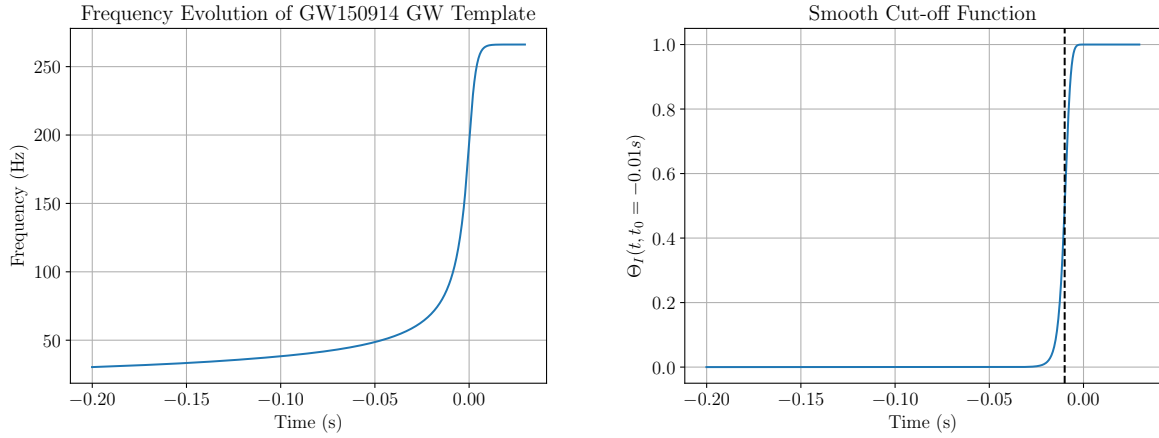
(a) The frequency evolution $\omega_I(t)$ of the IMR tem-
plate

(b) The smooth cut-off function $\Theta(t, t_0)$. The dashed
vertical line is $t = t_0$.

Figure 6: (6a) The frequency evolution of the best-fit IMR template for GW150914. (6b) The smooth cut-off function to be applied to GW150914 IMR template to generate the echo template.
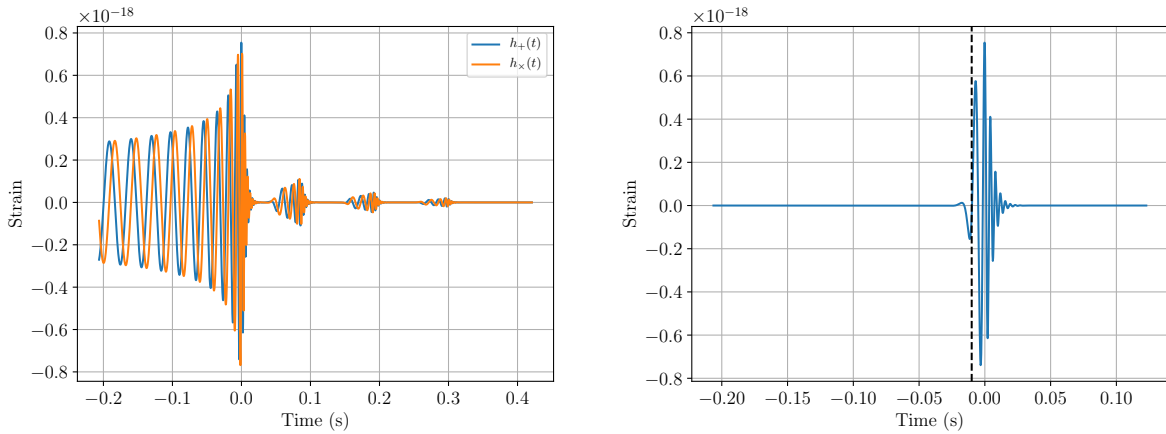
(a) GW150914 best-fit IMR waveform with three
echoes appended

(b) The truncated IMR waveform $\mathcal{M}_{T,I}(t)$ used to
produced the echo template

Figure 7: (7a) The best-fit IMR template for GW150914 with three echoes appended in the source frame. (7b) The truncated IMR waveform $\mathcal{M}_{T,I}(t)$ used to generate the echo template.

where F_+, $F_\times$ are the detector responses for plus and cross polarization respectively, and α, δ and ψ are the right ascension, declination of the source, polarization of the gravitational wave respectively.

Figure 8a shows the 10-second long of strain of pure Gaussian noise in H1, with lower frequency cut-off $f_{\text{low}} = 30$ Hz. Figure 8b shows the 10-second long strain of Gaussian noise with an IMRE signal injected in H1 at geocentric GPS time $t_{\text{merger}} = 1126259462.430$ s, with the same lower frequency cut-off. We can observe from Figure 8b that only the merger part of the signal stands out from the noise floor.

(a) The strain of pure Gaussian noise in H1

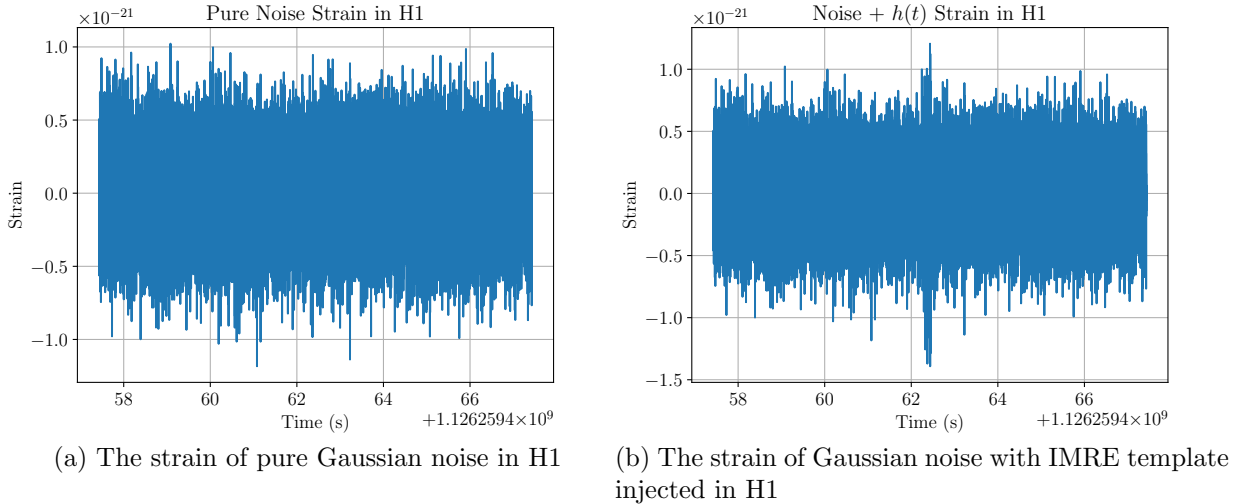(b) The strain of Gaussian noise with IMRE template injected in H1

Figure 8: The fake strain in H1 generated for the analysis. An IMRE signal was injected at geocentric GPS time $t_{\text{merger}} = 1126259462.430$ s. We can see from Fig 8b that the signal stands out from the noise floor.

3.2.2 Parameter estimation on fake strain data

This is a work in progress. Currently the parameter estimation program is running on LIGO cluster.

4 Acknowledgements

References

[1] B. P. Abbott, R. Abbott, T. D. Abbott, M. R. Abernathy, F. Acernese, K. Ackley, C. Adams, T. Adams, P. Addesso, R. X. Adhikari, and et al. Tests of General Relativity with GW150914. *Physical Review Letters*, 116(22):221101, June 2016.

[2] B. P. Abbott et al. Gw151226: Observation of gravitational waves from a 22-solar-mass binary black hole coalescence. *Phys. Rev. Lett.*, 116:241103, Jun 2016.

[3] B. P. Abbott et al. Observation of gravitational waves from a binary black hole merger. *Phys. Rev. Lett.*, 116:061102, Feb 2016.

[4] B. P. Abbott et al. Gw170104: Observation of a 50-solar-mass binary black hole coalescence at redshift 0.2. *Phys. Rev. Lett.*, 118:221101, Jun 2017.

[5] J. Abedi, H. Dykaar, and N. Afshordi. Echoes from the Abyss: Evidence for Planck-scale structure at black hole horizons. *ArXiv e-prints*, December 2016.

[6] J. Abedi, H. Dykaar, and N. Afshordi. Echoes from the Abyss: The Holiday Edition! *ArXiv e-prints*, January 2017.

[7] G. Ashton, O. Birnholtz, M. Cabero, C. Capano, T. Dent, B. Krishnan, G. D. Meadors, A. B. Nielsen, A. Nitz, and J. Westerweck. Comments on: "Echoes from the abyss: Evidence for Planck-scale structure at black hole horizons". *ArXiv e-prints*, December 2016.

[8] V. Cardoso, E. Franzin, and P. Pani. Is the Gravitational-Wave Ringdown a Probe of the Event Horizon? *Physical Review Letters*, 116(17):171101, April 2016.

[9] V. Cardoso, S. Hopper, C. F. B. Macedo, C. Palenzuela, and P. Pani. Gravitational-wave signatures of exotic compact objects and of quantum corrections at the horizon scale. *Physical Review D*, 94(8):084031, October 2016.

[10] Jolien D. E. Creighton and Warren G. Anderson. Gravitational-wave physics and astronomy : an introduction to theory, experiment and data analysis / Jolien D.E. Creighton and Warren G. Anderson. page 269, 2011.

[11] Tito Dal Canton et al. Implementing a search for aligned-spin neutron star-black hole systems with advanced ground based gravitational wave detectors. *Phys. Rev.*, D90(8):082004, 2014.

[12] D. Foreman-Mackey, D. W. Hogg, D. Lang, and J. Goodman. emcee: The MCMC Hammer. *Publications of the Astronomical Society of the Pacific*, 125:306, March 2013.

[13] Paul M. Goggans and Ying Chi. Using thermodynamic integration to calculate the posterior probability in bayesian model selection problems. *AIP Conference Proceedings*, 707(1):59–66, 2004.

[14] W. K. Hastings. Monte carlo sampling methods using markov chains and their applications. *Biometrika*, 57(1):97–109, 1970.

[15] Tjonnie G F Li. *Extracting Physics from Gravitational Waves Testing the Strong-field Dynamics of General Relativity and Inferring the Large-scale Structure of the Universe.* Springer International Publishing, 1 edition, 2015.

[16] Michele Maggiore. Gravitational Waves Volume 1: Theory and Experiments. page 351, 2008.

[17] Z. Mark, A. Zimmerman, S. M. Du, and Y. Chen. A recipe for echoes from exotic compact objects. *ArXiv e-prints*, June 2017.

[18] Nicholas Metropolis and S. Ulam. The monte carlo method. *Journal of the American Statistical Association*, 44(247):335–341, 1949.

[19] H. Nakano, N. Sago, H. Tagoshi, and T. Tanaka. Black hole ringdown echoes and howls. *ArXiv e-prints*, April 2017.

[20] Robert H. Swendsen and Jian-Sheng Wang. Replica monte carlo simulation of spin-glasses. *Phys. Rev. Lett.*, 57:2607–2609, Nov 1986.

[21] Samantha A. Usman et al. The PyCBC search for gravitational waves from compact binary coalescence. *Class. Quant. Grav.*, 33(21):215004, 2016.